International Journal of GEOMATE, Sept. 2023, Vol. 25, Issue 109, pp.1-8
ISSN: 2186-2982 (P), 2186-2990 (O), Japan, DOI: https://doi.org/10.21660/2023.109.3947
Geotechnique, Construction Materials and Environment

# NONLINEAR BENDING ANALYSIS OF FGM BEAMS UNDER VARIOUS BOUNDARY CONDITIONS BY RITZ METHOD

*Xuan-Hung Dang[1]

[1]Faculty of Building and Industrial Construction, Hanoi University of Civil Engineering (HUCE), Vietnam

*Corresponding Author, Received: 12 May 2023, Revised: 25 May 2023, Accepted: 2 June 2023

ABSTRACT: This paper deals with the nonlinear bending response of functionally graded beams (FG beams) with various boundary conditions using the Ritz method. The displacement components are developed in a series of increasing-order polynomials (Pb-Ritz) that satisfy the geometric boundary conditions. The bending beam model is built based on a high-order shear deformation beam theory, considering the von Kárman type of geometrical nonlinearity strains. First, the potential energies of internal and external forces are determined. The system of nonlinear governing equations is then derived using the minimum total potential energy principle. The Newton-Raphson iterative algorithm is used to solve this system of nonlinear equations. The convergence test and the validated example are conducted by comparing them with the available published results to show the accuracy of the obtained results. Parametric studies are also performed to clarify the effect of the material properties, geometric parameters, boundary conditions, and nonlinearity on the displacement and stress fields of the beam.

*Keywords: FGM beam, Nonlinear bending, Pb-Ritz method, Shear deformation beam theory*

## 1. INTRODUCTION

Geometrically nonlinear bending analysis of beams is of great interest to researchers worldwide, especially those composed of new materials like composites or functionally graded materials. In 2009, Kang et al. [1] studied the bending of an FGM cantilever beam subjected to an end force, considering the exact neutral surface position and the nonlinear stress-strain relationship of the Ludwick-type law. This paper used the analytical method to study the effect of material parameters and nonlinearity on the displacement and stress fields of the beam. Therefrom, they concluded that the FGM beam might bear a larger applied load than the homogeneous one if we choose a reasonable volume fraction index for the FGM material and the bending tensile stress reaches its maximum at an internal point rather than at the surfaces, as in the homogeneous beam. These authors, in 2010, extended this problem to an FGM cantilever beam subjected to an end moment [2]. In this paper, besides the study on the effect of the large deformation, the authors also optimized the volume fraction index of the FGM material in order to obtain a lighter weight and a larger stiffness beam. The exact neutral surface position and geometrical nonlinearity of the FGM beams were also studied by Zhang et al. [3] using high-order shear deformation beam theory and the Ritz method. The authors indicated that the neutral surface position will change with temperature and have to be considered in the study. Akbas et al., in 2013, used the finite element method to analyze the geometric nonlinearity of an FGM edge cracked cantilever Timoshenko beam subjected to a transversal point load at the free end [4]. In which the cracked beam is modeled as an assembly of two sub-beams connected through a massless elastic rotational spring. This author, in 2020, published one more study on the geometrically nonlinear analysis of an axially functionally graded beam using the finite element method [5]. Wan et al. in [6] paid their attention to the geometric nonlinearity of the FGM Timoshenko curved beams with variable curvatures, in which the axial extension, the transversal shear deformation, and the geometric nonlinearity were simultaneously considered.

Many other researchers paid attention to the effect of thermal loading on the geometrically nonlinear behavior of the FGM beams. For example, in 2011, Ma et al. published a further discussion of nonlinear mechanical behavior for FGM beams under in-plane thermal loading [7]. Based on the first-order shear deformation beam theory and analytical method, the authors indicated that due to the variation of the material properties through the thickness, bifurcation buckling cannot occur for simply supported beams, and while subjected to in-plane thermal loading, the FGM beam will exhibit some interesting characteristics. An exact solution for the same problem was developed by these authors in [8]. Ghiasian et al., in their paper [9], studied the simultaneous effect of rapid heating and geometric nonlinearity on the behavior of FGM beams. Abkas et al., one more time, published a study on the effect of hygro-thermal loading on the nonlinear behavior of FGM cantilever beams [10].

The influence of an elastic foundation was also considered in the nonlinear analysis of FGM beams [11] or in combination with the effect of the thermal environment in [12]. Recently, many investigations have been focused on the nonlinear behavior of functionally graded porous beams (FGP beams), in which the porosity varies continuously through the thickness. Among them, it is necessary to mention the studies of Chen et al. [13] on the buckling and static bending of FGP beams, of Wattanasakulpong et al. [14] on the vibration of FGP beams, and of Phuong et al. [15] on the bending of FGP beams including the effect of neutral surface position and elastic foundation. An overview of the modeling and analysis of FGM structures was also presented by Gupta et al. [16].

The above-mentioned studies addressed many different problems with various beam models and computational methods, in which different types of boundary conditions and external loading were considered. However, in-depth analysis of the effects of geometric nonlinearity, material properties, dimensional parameters, and boundary conditions has not been fully addressed. This paper aims to provide a detailed analysis of the load-deflection curve and the distribution law of the stress components along the thickness of FGM beams under the influence of external factors. Section 3 presents the model of the nonlinear bending FGM beam; the convergence test and validation of the obtained results are undertaken in Section 4; Section 5 indicates the parametric studies of the input parameters on the load-deflection curve and the distribution law of the stress components along the thickness; and finally, the conclusions are presented in Section 6.

## 2. RESEARCH SIGNIFICANCE

The nonlinear behavior analysis of the structure made of new materials, such as FGM or FGP material, is essential for its design and application. This paper aims to provide a detailed analysis of the load-deflection curve and the distribution law of the stress components along the thickness of a FGM beam under the influence of material properties, boundary conditions, length-to-thickness ratio, and von Karman nonlinearity.

## 3. MODEL OF A NONLINEAR BENDING FGM BEAM

### 3.1 Functionally Graded Material (FGM)

Consider a FGM beam of dimension $L \times h \times b$ and the system of coordinates as in Fig. 1. The FGM is composed of metal and ceramic, in which the volume fraction varies continuously through the thickness according to a law represented by function $V(z)$. Therefore, the material properties of the FGM at any point within the beam are determined by.

$$H(z) = V_m(z) H_m + V_c(z) H_c \quad (1)$$

where $H_c$ and $H_m$ are the material properties of ceramic and metal, respectively, $V_c(z)$ and $V_m(z)$ are corresponding volume fractions of each component and $V_c(z) + V_m(z) = 1$. In this study, the volume fraction function $V_c(z)$ is assumed to be according to the power law.

$$V_c(z) = \left( \frac{1}{2} + \frac{z}{h} \right)^p, \quad z \in [-h/2, h/2] \quad (2)$$

with $p$ is the volume fraction index of the FGM and $p \geq 0$.

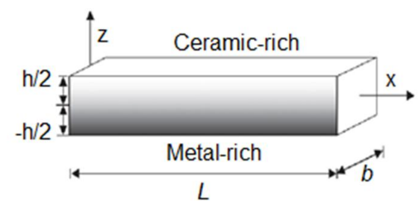


Fig. 1 FGM beam composed of ceramic and metal

Fig. 2 shows the variation of the elastic modulus of the FGM through the thickness with various volume fraction indices. It is obvious that when the volume fraction index $p$ tends to 0, the volume fraction of the ceramic tends to 1, and the material is purely ceramic. Inversely, when $p$ tends to be infinite, the volume fraction of the ceramic tends to 0 and the material is purely metal. When $p = 1$, the power law becomes the linear law, the elastic modulus linearly varies.

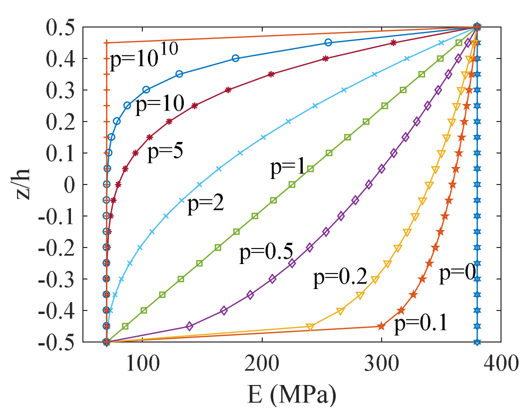


Fig. 2 Elastic modulus of FGM with various volume fraction indices

### 3.2 High-Order Shear Deformation Beam Theory

The high-order shear deformation theory of Reddy [17] is used to build the bending FGM beam model. The displacement field of a point within the beam is written by.

$$\begin{aligned} u(x,z) &= u_0(x) - z w_{0,x} + f(z)\theta_x(x) \\ w(x,z) &= w_0(x) \end{aligned} \tag{3}$$

where $u_0, w_0$ are the displacement components of a point in the mid-plan in the $x, z$ directions, respectively, $\theta_x$ is the slope of the transverse normal at $z = 0$ that represents the shear deformation about the $y$ axis, the operator (,) denotes the time derivative of a function, and $f(z)$ is the representative function of the theory.

$$f(z) = z\left[1 - \frac{4}{3}\left(\frac{z}{h}\right)^2\right] \tag{4}$$

The strain field from the kinematic equations incorporating nonlinear strain components according to von Karman's assumptions is stated as follow:

$$\begin{aligned} \varepsilon_x &= u_{0,x} - z w_{0,xx} + f(z)\theta_{x,x} + \frac{1}{2} w_{0,x}^2 \\ \gamma_{xz} &= f_{,z}(z)\theta_x \end{aligned} \tag{5}$$

The stress components in the beam are determined by Hooke's law.

$$\begin{Bmatrix} \sigma_{xx} \\ \sigma_{xz} \end{Bmatrix} = \begin{pmatrix} C_{11} & 0 \\ 0 & C_{66} \end{pmatrix} \begin{Bmatrix} \varepsilon_{xx} \\ \gamma_{xz} \end{Bmatrix} \tag{6}$$

where:

$$C_{11} = \frac{E(z)}{1 - \nu_z^2} \qquad C_{66} = G(z) = \frac{E(z)}{2(1 + \nu_z)} \tag{7}$$

with $\nu_z$ is the Poisson's ratio that is assumed to be constant through the thickness.

The elastic potential energy of the beam is determined by.

$$U = \frac{1}{2}\int_S \int_0^L \left(\sigma_{xx}\varepsilon_{xx} + \sigma_{xz}\gamma_{xz}\right) dS\, dx \tag{8}$$

Introducing (5), (6) and (7) into (8), one obtains.

$$\begin{aligned} U &= \frac{1}{2}\int_S \int_0^L \left(\sigma_{xx}\varepsilon_{xx} + \sigma_{xz}\gamma_{xz}\right) dS\, dx \\ &= \frac{1}{2}\int_0^L \begin{pmatrix} A u_{0,x}^2 + D w_{0,x}^2 + H^* \theta_{x,x}^2 \\ +0.25 A w_{0,x}^4 + 2B u_{0,x} w_{0,xx} \\ +2B^* u_{0,x}\theta_{x,x} + A u_{0,x} w_{0,x}^2 \\ +2D^* w_{0,xx}\theta_{x,x} + B w_{0,xx} w_{0,x}^2 \\ +B^* \theta_{x,x} w_{0,x}^2 \end{pmatrix} dx \\ &+ \frac{1}{2}\int_0^L \left(A^* \theta_x^2\right) dx \end{aligned} \tag{9}$$

where the stiffness components are determined by.

$$\begin{aligned} A &= b\int_{-h/2}^{h/2} E(z)\,dz \\ B &= b\int_{-h/2}^{h/2} -zE(z)\,dz \\ D &= b\int_{-h/2}^{h/2} z^2 E(z)\,dz \\ A^* &= b\int_{-h/2}^{h/2} f_{,z}^2(z) G(z)\,dz \\ B^* &= b\int_{-h/2}^{h/2} f(z)E(z)\,dz \\ D^* &= b\int_{-h/2}^{h/2} -zf(z)E(z)\,dz \\ H^* &= b\int_{-h/2}^{h/2} f^2(z)E(z)\,dz \end{aligned} \tag{10}$$

The potential energy of external loads $V$ on a beam subjected to a uniformly distributed load $q_0$ is written as follows:

$$V = -b\int_0^L q_0 w_0\, dx \tag{11}$$

The total potential energy of the beam is determined by.

$$\Pi = U + V \tag{12}$$

### 3.3. Pb-Ritz Method

The Pb-Ritz method is based on the expansion of the displacement components into a series of algebraic functions that satisfy the boundary conditions [18].

$$\begin{aligned} & u_0(x) = \sum_{i=1}^{n} c_i \varphi_i \;\; ; \;\; w_0(x) = \sum_{j=1}^{n} d_j \psi_j \\ & \theta_x(x) = \sum_{k=1}^{n} e_k \phi_k \end{aligned} \tag{13}$$

where $c_i$ , $d_j$ , $e_k$ are the unknown coefficients that need to be determined, and $\varphi_i$ , $\psi_j$ , $\phi_k$ are the admissible functions in the form of increasing order polynomials, and $n$ is the number of terms in the expansion.

$$\begin{aligned} & \varphi_i = f_u\, x^{i-1}; \quad \psi_j = f_w\, x^{j-1}; \quad \phi_k = f_\theta\, x^{k-1} \\ & (i\ ,\ j\ ,\ k = 1, 2, ..., n) \end{aligned} \tag{14}$$

with $f_* = x^{p_*}(L - x)^{q_*}$ and $p_*$, $q_*$ are the boundary condition representative coefficients as in Table 1 ($* = u, w, \theta$).

Apply the principle of minimum total potential energy, the stationary condition of the total potential energy yields.

$$\frac{\partial \Pi}{\partial c_i}=0\ ;\ \frac{\partial \Pi}{\partial d_j}=0\ ;\ \frac{\partial \Pi}{\partial e_k}=0 \quad (i,j,k=1,...,n) \tag{15}$$

The system of nonlinear equations (15) is solved using the Newton-Raphson iterative algorithm.

Table 1 Boundary condition representative coefficients (Clamped: C; Hinged: H; Free: F)

| BCs | C-C | H-H | C-F | C-H |
|---|---|---|---|---|
| $p_u$ | 1 | 1 | 1 | 1 |
| $q_u$ | 1 | 1 | 0 | 1 |
| $p_w$ | 2 | 1 | 2 | 2 |
| $q_w$ | 2 | 1 | 0 | 1 |
| $p_\theta$ | 1 | 0 | 1 | 1 |
| $q_\theta$ | 1 | 0 | 0 | 0 |

## 4. CONVERGENCE AND VALIDATION

### 4.1 Input Parameters

Consider an FGM beam with input parameters as follows:

Dimensions: length $L$, width $b$, thickness $h$;

Boundary conditions: Clamped-Clamped (CC), Simply supported ends (SS), Clamped - Simply supported (CS) and Clamped - Free (CF) ;

Properties of the metal and ceramic:

Ceramic ($Al_2O_3$): $E_c=380$ GPa, $\nu_c=0.3$.

Metal (Al): $E_m=70$ GPa, $\nu_m=0.3$.

Uniformly distributed load $q_0$.

In the following tests, the dimensionless quantities are used :

+ Dimesionless deflection.

$$\bar{w}=\frac{w_0(L/2)}{h} \tag{16}$$

+ Dimesionless stresses:

$$\sigma_x^*(z)=\frac{h}{q_0L}\sigma_x\left(\frac{L}{2},z\right);\ \tau_{xz}^*(z)=\frac{h}{q_0L}\tau_{xz}(0,z) \tag{17}$$

+ Dimensionless load:

$$P=\frac{q_0L^4}{E_mh^4} \tag{18}$$

### 4.2 Convergence Test

Due to the expansion in a series of increasing order polynomials (13), the obtained results reach convergence only when the number of terms in the expansion $n$ is sufficiently large. Consider a FGM beam with $L/h=20$, $p=5$, $P=30$, various boundary conditions (CC, SS, CF, CS) and the various numbers of terms in the expansion $n=1\div 9$. The obtained maximum dimensionless deflections are listed in Table 2. It is obvious that dimensionless deflection rapidly reaches convergence as soon as $n=6$. However, $n=9$ is used in the following tests to obtain exact results.

Table 2: Convergence of the maximum dimensionless deflection when the number of terms in the expansion increases $(L/h=20\ ;\ p=5)$

| n | CC | SS | CF | CS |
|---|---|---|---|---|
| 2 | 0.4493 | 0.6252 | 10.7870 | 0.5829 |
| 3 | 0.4528 | 0.6974 | 16.4297 | 0.5966 |
| 4 | 0.4647 | 0.7077 | 24.6656 | 0.6050 |
| 5 | 0.4664 | 0.7047 | 25.2741 | 0.6071 |
| 6 | 0.4694 | 0.7047 | 25.2790 | 0.6087 |
| 7 | 0.4694 | 0.7048 | 25.2799 | 0.6091 |
| 8 | 0.4693 | 0.7048 | 25.2806 | 0.6089 |
| 9 | 0.4693 | 0.7048 | 25.2811 | 0.6089 |

### 4.3 Validation

The validation of the obtained results will be performed by comparing them with those in [19] and [20], in which the analytical and Ritz methods were utilised. Consider a homogeneous beam of aluminium with input parameters $E$ = 70 GPa, $\nu$ = 0.3, $h$ = 0.1m, and $L/h$ = 20, subjected to a uniformly distributed load $q_0$ and boundary conditions SS, CC. Table 3 shows the maximum dimensionless deflection $\bar{w}=\frac{w_{0\max}}{h}$ with various dimensionless load levels $P=\frac{q_0L^4}{Eh^4}$.

It can be observed that there is a good agreement between the obtained results and those in the references for all boundary conditions and all levels of load. The maximum error is only 0.79% for the case *P = 120* and the boundary condition CC. This justifies the accuracy of the obtained results.

Table 3 Nonlinear bending of a homogeneous beam with various boundary conditions

| | | P | | | |
|---|---|---|---|---|---|
| | | 1 | 8 | 30 | 80 |
| SS | [20] | 0.1474 | 0.5980 | 1.0530 | 1.5150 |
| | [19] | 0.1474 | 0.5979 | 1.0532 | 1.5142 |
| | This paper | 0.1474 | 0.5979 | 1.0531 | 1.5142 |
| CC | [20] | 0.0321 | 0.2460 | 0.7042 | 1.2210 |
| | [19] | 0.0322 | 0.2467 | 0.7067 | 1.2273 |
| | This paper | 0.0321 | 0.2463 | 0.7054 | 1.2240 |

## 5. PARAMETRIC STUDIES

### 5.1. Distribution of The Stress Components Through The Beam's Thickness

The distributions of the dimensionless stress components through the thickness of a FGM beam (SS, *L/h* = 20, *P* = 30) with various volume fraction indices ( $p = 0.0,\ 0.5,\ 1.0,\ 5.0$ ) are shown in Fig. 3 and Fig. 4. When *p* = 0, the FGM is purely ceramic and hence the normal stress distribution is linear and the shear stress one is parabolic through the thickness. However, the normal stress distribution is not symmetric via the mid-plane. The value of the tension stress is higher than that of the compression stress.

The equations (5), (6), and (7) show that the normal stress depends on $z^3$, while the shear stress is solely determined by $z^2$. Thus, it seems that the distribution law of shear stress is reasonable, but that of normal stress is not. This indicates that the contribution of the term $f(z)\theta_{x,x}$ in equation (5) is not significant. On the other hand, the term $\frac{1}{2}w_{0,x}^2$ in equation (5) is always positive and constant through the thickness, which hence moves the diagram of normal stress to the right so that it is not still symmetric. Moreover, due to this term $\frac{1}{2}w_{0,x}^2$, an axial force appears in the beam that causes an arch effect, which makes the deflection in the nonlinear analysis less than that in the linear one.

The distribution law of the normal stress of the pure ceramic beam (*p* = 0) indicates that the axial strain $\varepsilon_x$ is linear through the thickness. When the volume fraction index is not equal to zero, the volume fractions of constituent materials vary according to the power law (2); thus, stress components distribute nonlinearly through the height direction of the beams, and their forms depend on the value of the volume fraction index. Normal stress does not reach the extreme values on the top and bottom surfaces of the beams like a homogeneous beam's behavior (*p* = 0.5).

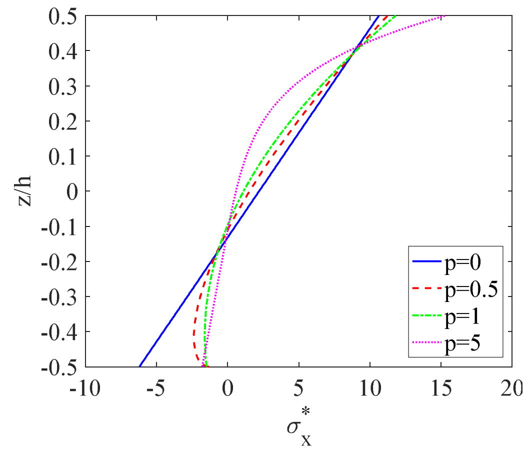


Fig. 3 Distribution of the dimensionless normal stress through the beam's thickness

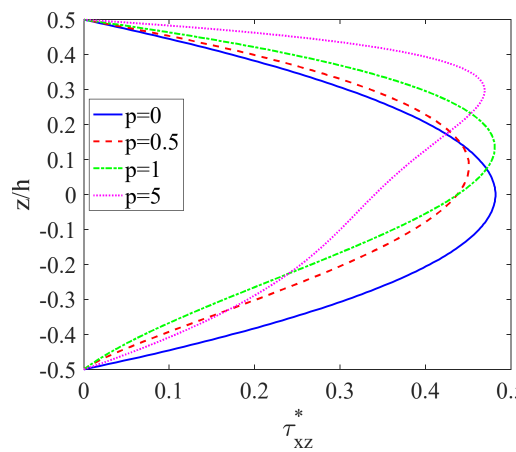


Fig. 4 Distribution of the dimensionless shear stress through the beam's thickness

### 5.2. Effect of Boundary Conditions

A FGM beam with input parameters *L/h* = 20, $p$ = 5, subjected to various levels of dimensionless uniformly distributed load $P = 0 \div 50$ and with various boundary conditions (CC, SS, CF and CS). The dimensionless deflection test results are listed in Table 4 and graphically presented in Fig. 5.

It can be seen that while the load-deflection curves of the CC, SS and CS boundary conditions are nonlinear, the CF one seems not to be. It separates from the others and its values are much higher than the others' corresponding ones (Table 4). This phenomenon indicates that there is no nonlinear effect in the CF beam.

One knows that the nonlinear effect is due to the apparition of the axial strain $\frac{1}{2}w_{0,x}^2$, but the free end of the CF beam does not prevent this deformation, so there is no stretching of mid-plane and therefore the axial force is zero.

Table 4 Maximum dimensionless deflection of a FGM beam with various boundary conditions and load levels

| $P$ | Boundary conditions | | | |
|---|---|---|---|---|
| | CC | SS | CF | CS |
| 0 | 0.0000 | 0.0000 | 0.0000 | 0.0000 |
| 10 | 0.1774 | 0.3903 | 8.4271 | 0.2886 |
| 20 | 0.3355 | 0.5752 | 16.8541 | 0.4738 |
| 30 | 0.4693 | 0.7048 | 25.2811 | 0.6089 |
| 40 | 0.5825 | 0.8072 | 33.7080 | 0.7165 |
| 50 | 0.6798 | 0.8932 | 42.1349 | 0.8068 |

The load-deflection curves have different levels of nonlinearity that increase in the order CC, CS and SS, in which the CC curve seems approximatively linear. Moreover, in the same order, the values of deflection also increase. So, the nonlinearity level augments with the deflection of the beam. This shows good agreement with the logical analysis that indicates that the CC boundary conditions make the beam stiffer than the CS one, which is stiffer than the SS one.

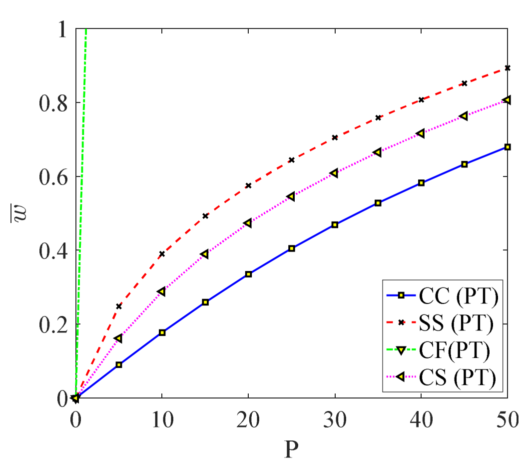


Fig. 5 Load-deflection curve of a FGM beam with various boundary conditions

### 5.3. Effect of Volume Fraction Index

A FGM beam with input parameters $L/h = 20$, $p = 0.0, 0.5, 1.0, 5.0$ and boundary condition SS, subjected to uniformly distributed load $P = 0 \div 50$. The corresponding maximun dimensionless deflections of the beam are presented in Table 5 and on Fig. 6.

Table 5 Maximum dimensionless deflections of the FGM beam with various volume fraction indices

| $P$ | Volume fraction index $p$ | | | |
|---|---|---|---|---|
| | 0 | 0.5 | 1 | 5 |
| 0 | 0.0000 | 0.0000 | 0.0000 | 0.0000 |
| 10 | 0.2448 | 0.2805 | 0.3024 | 0.3903 |
| 20 | 0.3930 | 0.4280 | 0.4546 | 0.5752 |
| 30 | 0.4952 | 0.5310 | 0.5616 | 0.7048 |
| 40 | 0.5743 | 0.6121 | 0.6462 | 0.8072 |
| 50 | 0.6396 | 0.6798 | 0.7171 | 0.8932 |

According to Fig. 6, it can be observed that as the volume fraction index increases, both the deflection and the level of nonlinearity also increase. We know that when $p = 0$ the beam is purely ceramic that is much stiffer than the metal. The volume fraction of the metal increases with the volume fraction index. Therefore, the augmentation of the volume fraction index makes the beam softener. As a result, the deflection and the nonlinearity level increase.

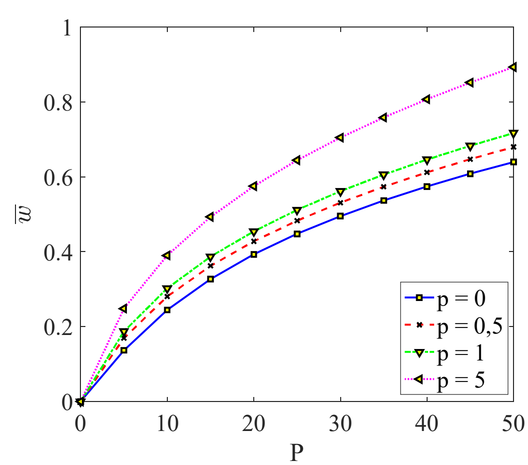


Fig. 6 Load-deflection curves of the FGM beam with various volume fraction indices

### 5.4. Effect of Length-to-Thickness Ratio

A FGM beam (SS, $p$ = 5) subjected to a uniformly distributed load $q_0 = 0 \div 20$ (MPa) with various length-to-thickness ratios $\frac{L}{h} = 5;10;20;30$. The maximum dimensionless deflections of the beam are listed in Table 6 and the load-deflection curves are presented in Fig. 7. It is obvious that the longer the beam, the larger the deflection. For the short beams ( $L/h = 5;10$ ), the obtained deflections are too small, thus the nonlinearity level seems to be zero. The load-deflection curves are approximately linear. The nonlinearity only appears in the case of long beams $L/h = 20;30$, in which the deflections are large enough. It also indicated that the larger the deflection, the stronger the nonlinearity. This clarifies that the geometric nonlinearity is due to the large deformation.

Table 6 Maximum dimensionless deflection of the FGM beam with various length-to-thickness ratios

| $q_0$ (MPa) | Length-to-thickness ratio $L/h$ | | | |
|---|---|---|---|---|
| | 5 | 10 | 20 | 30 |
| 0 | 0.0000 | 0.0000 | 0.0000 | 0.0000 |
| 4 | 0.0030 | 0.0407 | 0.3696 | 0.8618 |
| 8 | 0.0059 | 0.0771 | 0.5488 | 1.1620 |
| 12 | 0.0088 | 0.1099 | 0.6747 | 1.3693 |
| 16 | 0.0117 | 0.1397 | 0.7744 | 1.5326 |
| 20 | 0.0146 | 0.1669 | 0.8580 | 1.6697 |

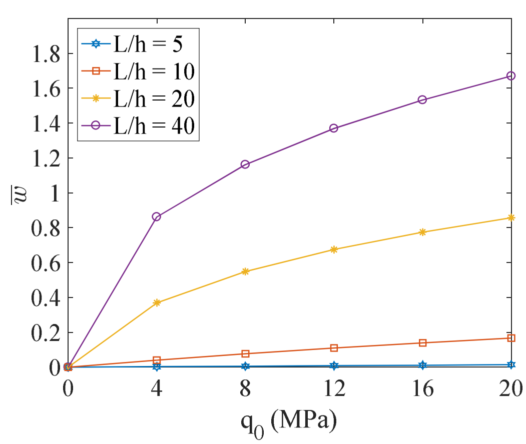


Fig. 7 Load-deflection curves of the FGM beam with various length-to-thickness ratios

## 6. CONCLUSIONS

The geometric nonlinear analysis of a FGM beam with various boundary conditions subjected to a uniformly distributed load is studied. The effects of the input parameters on the deflection and the stress components are analyzed in detail. The von Karman nonlinear strain component causes the stretching of the mid-plane. Once the boundary conditions prevent this stretching, an axial force will appear and cause an arch effect, which makes the deflection in the nonlinear analysis smaller than that in the linear one. Therefore, the von Karman nonlinear type does not appear in the cantilever beams. It is found that the larger the deflection, the stronger the nonlinearity level. When the stiffness of the beam is too high or the applied load is too small, the large deformation theory approximates the small deformation theory. The distribution laws of stress components depend on the deformation and material property distributions and become nonlinear. In the extremum case, when the FGM is pure ceramic, the normal stress is linear through the thickness and asymmetric via the mid-plane, while the shear stress is parabolic. It is the nonlinear effect that moves the normal stress diagram to the right and causes its asymmetric form.

## 7. REFERENCES

[1] Kang Y.A. and Li X.F., Bending of functionally graded cantilever beam with power-law nonlinearity subjected to an end force. International Journal of Nonlinear Mechanics, 44, 2009, pp. 696-703.
[2] Kang Y.A. and Li X.S., Large Deflection of Nonlinear Cantilever Functionally Graded Beam. Journal of Reinforced Plastics and Composites, Vol 29, 2010, pp. 1761-1774.
[3] Zhang D.G., Nonliear bending analysis of FGM beams based on physical neutral surface and high order shear deformation theory. Composite Structures, 100, 2013, pp. 121-126.
[4] Akbas S.D., Geometrically Nonlinear Static Analysis of Edged Cracked Timoshenko Beams Composed of Functionally Graded Material. Mathematical Problems in Engineering, Vol 2013, 2013, pp. 1-14.
[5] Akbas S.D., Geometrically nonlinear analysis of axially functionally graded beams using finite element method. J. Appl. Comput. Mech., Vol. 51, No. 2, 2020, pp. 411-416.
[6] Wan Z.Q., Li S.R. and Ma H.W., Geometrically Nonlinear Analysis of Functionally Graded Timoshenko Curved Beams with Variable Curvatures. Advances Mater. Sci. and Eng., Vol. 2019, 2019, pp. 1-10.
[7] Ma L.S. and Lee D.W., A futher discussion of nonlinear mechanical behavior for FGM beams

under in-plane thermal loading. Composite Structures, Vol. 93, 2011, pp. 831-842.

[8] Ma L.S. and Lee D.W., Exact solutions for nonlinear static responses of a shear deformable FGM beam under an in-plane thermal loading. Euro. J. Mech. A/Solids, Vol. 31, 2012, pp. 13-20.

[9] Ghiasian S.E., Kiani Y. and Eslami M.R., Nonlinear rapid heating of FGM beams. International Journal of Nonlinear Mechanics, 67, 2014, pp. 74-78.

[10] Akbas S.D., Hygro-Thermal Analysis of a Functionally Graded Beam. J. Appl. Comput. Mech., 5(2), 2019, pp. 477-485.

[11] Li Q.L. and Shao Q.H., Nonlinear Analysis of a FGM Cantilever Beam Supported on a Winkler elastic foundation. Applied Mechanics and Materials, Vol 602-605, 2014, pp. 131-134.

[12] Shen H.S. and Wang Z.X., Nonlinear analysis of shear deformable FGM beams resting on elastic foundation in thermal environments. Int. J. Mech. Sci., 81, 2014, pp. 195-206.

[13] Chen D., Yang J. and Kitipornchai S., Elastic buckling and static bending of shear deformable functionally graded porous beam. Composite Structures, 133, 2015, pp. 54-61.

[14] Wattanasakulpong N., Chaikittiratana A. and Pornpeerakeat S., Chebyshev collocation approach for vibration analysis of functionally graded porous beams based on third-order shear deformation theory. Acta Mechanica Sinica, 34(6), 2018, pp. 1124-1135.

[15] Phuong N.T.B., Tu T.M. and Phuong H.T., Bending analysis of functionally graded beam with porosities resting on elastic foundation based on neutral surface position. Journal of Science and Technology in Civil Engineering (STCE)-NUCE, 13(1), 2019, pp. 33-45.

[16] Gupta A. and Talha M., Recent development in modeling and analysis of functionally graded materials and structures. Progress in Aerospace Sciences, 79, 2015, pp. 1-14.

[17] Reddy J.N., Mechanics of laminated composite plates- Theory and analysis (Book). Boca Raton, FL: CRC Press, 1997.

[18] Pradhan K. and Chakraverty S., Free vibration of Euler and Timoshenko functionally graded beams by Rayleigh–Ritz method. Composites Part B: Engineering, 51, 2013, pp. 175-184.

[19] Van Long N., Nguyen V.L. and Tran M.T., Exact solution for nonlinear static behaviors of functionally graded beams with porosities resting on elastic foundation using neutral surface concept. Proceedings of the Institution of Mechanical Engineers, Part C: Journal of Mechanical Engineering Science, 236(1), 2022, pp. 481-495.

[20] Zhangss D.G., Nonlinear bending analysis of FGM beams based on physical neutral surface and high order shear deformation theory. Composite Structures, 100, 2013, pp. 121-126.